Sensors & Diagnostics

COMMUNICATION

View Article Online
View Journal | View Issue

Cite this: *Sens. Diagn.*, 2025, **4**, 136

Received 28th August 2024,
Accepted 10th December 2024

DOI: 10.1039/d4sd00294f

rsc.li/sensors

Agarose-gel coating for improving the polydopamine-based pH sensor stability in continuous pH measurements†

Natalie Fudge, ‡[a] Fatemeh Keyvani,‡[a] Joshua Khatri[a] and Mahla Poudineh *[ab]

Continuous monitoring in healthcare could transform patient care by improving patient outcomes and reducing costs through rapid detection and timely intervention. The pH of body fluids is an essential indicator for detecting acid/base imbalances and subsequent diseases, as well as monitoring organ functions. However, current pH sensors experience signal drifts over continuous measurements, inhibiting their ability to provide longitudinal body's pH status. To enable real-time, continuous pH monitoring, we developed a polydopamine (PDA)-based pH sensor and validated its performance in PBS and simulated wound fluid exudate (WFE). To increase signal stability for continuous performance, heat treatment and agarose gel coating were applied to the sensor, and we observed that the agarose coating greatly improved the signal drift.

Introduction

The real-time data provided by continuous monitoring in healthcare settings has transformed patient care.[1–5] This advancement enables healthcare givers to rapidly detect changes in a patient's condition and provide necessary care, improving patient outcomes. In 1902, Willem Einthoven invented the first device to provide continuous monitoring of cardiac activity, the electrocardiogram (ECG).[6] In 1999, Medtronic became the first FDA-approved continuous glucose monitor (CGM), and since then, new methods have been explored to continuously measure crucial biomarkers and health indicators.[3] These innovations can potentially improve clinical outcomes,[5,7,8] reduce patient discomfort,[2,5] and decrease healthcare costs by minimizing hospital readmissions.[2]

The pH of body fluids, which measures the level of acidity or alkalinity of body fluids, can be linked to the development of diseases.[9] Particularly, pH measurements have been shown to be important in identifying infections,[5,10] monitoring wound healing processes,[5,11–13] and early detection of diseases.[5,10] Continuous pH monitoring can significantly improve patient care by quickly identifying pH trends, which can be utilized for prompt medical interventions.[2]

A variety of pH sensors have been developed, with most falling into the optical or electrochemical sensor categories.[5] Optical pH sensors undergo optical changes when interacting with hydrogen or hydroxide ions and generate optical or fluorescence signals, which are detectable *via* visual inspection.[5,14–16] While these pH sensors are cost-effective and offer a high signal-to-noise ratio, they are highly temperature-dependent and are prone to instability.[5,14] Conversely, electrochemical pH sensors utilize changes in electrochemical properties to measure ion concentration in response to changes in pH.[5,7,10,17–20]

The ion-sensitive field-effect transistor (ISFET) is the most common type of electrochemical pH sensor; however, it is subject to long-term drift and hysteresis, which can impact sensor accuracy, making it unsuitable for continuous measurement.[5,7,19,21] For example, a zirconium dioxide-gated ISFET pH sensor demonstrated a temporal drift of approximately 0.020 V over a 3 hour period.[22] Similarly, a baseline differential p-ISFET pH sensor experienced a drift of 0.018 V over 3 hours prior to the implementation of a drift correction mechanism.[23] Additionally, a hydrogenated amorphous silicon-gated ISFET was found to have a drift of 0.020 V during the same timeframe.[24] In contrast, our agarose-coated pH sensor exhibited a drift of only 0.011 V in PBS and 0.013 V in simulated wound fluid exudate (WFE) over a 3 hour test period, indicating an improvement over other conventional pH sensors. pH-Responsive materials such as poly (sodium 4-styrene sulfonate) (PSS)[17] and

[a] *Department of Electrical and Computer Engineering, Faculty of Engineering, University of Waterloo, Waterloo, ON N2L 3G1, Canada.*
E-mail: mahla.poudineh@uwaterloo.ca
[b] *Waterloo Institute for Nanotechnology, University of Waterloo, 200 University Ave. W, Waterloo, ON N2L 3G1, Canada*

† Electronic supplementary information (ESI) available. See DOI: https://doi.org/10.1039/d4sd00294f

‡ Authors contributed equally to the paper.

polyaniline (PANI),[17,18] in combination with nanoparticles, have been recently studied to create pH-sensing substrates.[5] These studies showed that these polymers exhibit a good Nernstian response (when the potential is linearly correlated with the logarithm of ionic activity) and typically offer a wider pH sensing range compared to ISFETs.[5,18,25] While cost-effective and sensitive, these sensors are also known to lack stability.[5]

Current methods used for pH sensing in health monitoring lack biocompatibility, sensitivity, and stability for continuous pH measurement.[5] To address this gap, we designed a polydopamine (PDA)-based pH sensor, verified its pH response, and improved its stability for continuous pH sensing. Fig. 1a, i represents the schematic of steps followed for fabricating the PDA-based pH sensor, and Fig. 1a, ii represents its sensing mechanism. PDA contains catechol moieties in its reduced form, which are oxidized to quinone moieties at a specific potential using cyclic voltammetry. As the pH increases, the potential at which this oxidation occurs decreases. This strong correlation between the PDA oxidation potential and pH value forms the basis of our pH sensor. Additionally, we examined two modifications, heat treatment and agarose gel coating, to enhance the durability of the pH sensor and evaluated their effectiveness (Fig. 1b). The drift in pH response over continuous scanning for the in-house fabricated PDA pH sensor was 60.8% in PBS and 75.0% in WFE, whereas the drift for the agarose-coated pH sensor was only 8.2% in PBS and 8.3% in WFE. Our findings suggest that the agarose coating effectively minimizes drift and achieves a stable signal over several continuous measurements.[4]

Experimental

Materials

The screen-printed gold electrodes (GSCL2W) were purchased from Conductive Technologies (York, PA, USA). 10× PBS was purchased from BioShop Canada (Burlington, ON, CA). Dopamine hydrochloride, agarose, hydrochloric acid (HCl), sodium hydroxide (NaOH), sulfuric acid (H_2SO_4), isopropanol (IPA), acetic acid, and other chemicals were purchased from Sigma Aldrich (Canada). Simulated wound fluid exudate (WFE) was purchased from Biochemazone (Leduc, Alberta, CA).

pH sensor fabrication

First, the gold electrodes were rinsed with isopropanol (IPA) and submerged for 10 minutes. Next, they were rinsed with MilliQ water and blotted with a KimWipe. The electrodes then underwent cleaning *via* ten cyclic voltammetry (CV) scans with a potential range between 0 V and 1.5 V at a scan rate of 0.1 V s^{-1} and a sampling interval of 0.005 V in 0.1 M H_2SO_4. The electrodes were thoroughly rinsed with MilliQ water and blotted with a KimWipe.

The following method is based on previously published protocols.[26,27] A 1 mg mL^{-1} solution of dopamine hydrochloride was prepared in 1× PBS and corrected to pH 7.4 using 0.5 M NaOH and 0.5 M HCl.[26,27] The dopamine was electropolymerized on the electrode surface under low light conditions *via* 30 CV cycles with a potential range between −0.5 V and 0.5 V at a scan rate of 0.05 V s^{-1} and a sampling interval of 0.005 V.[26,27] The PDA-coated pH sensors were

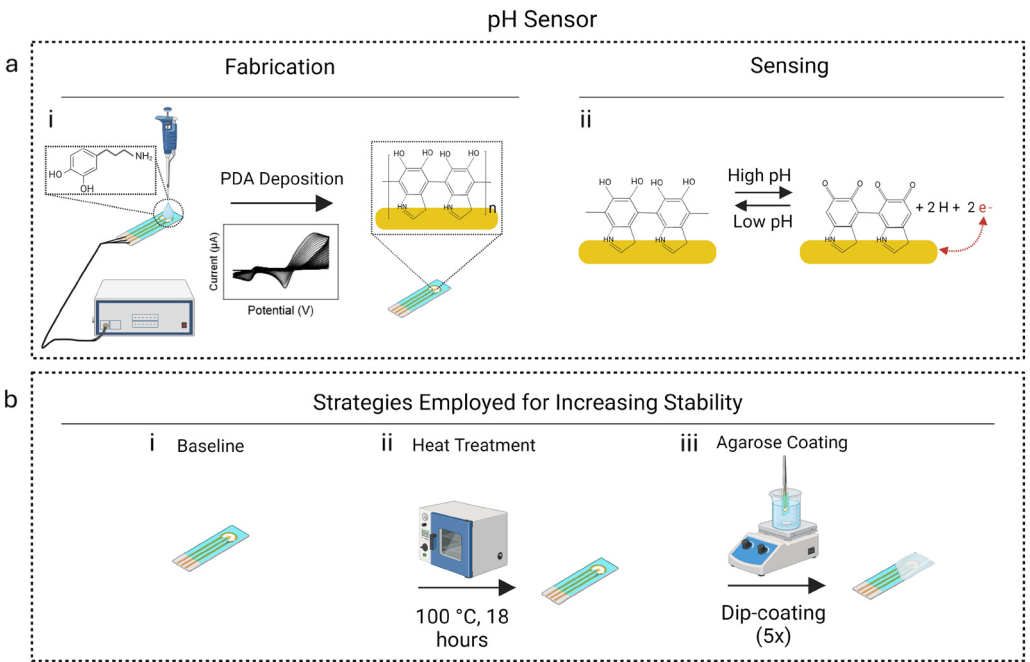

Fig. 1 Overview of the fabrication protocol and sensing mechanism of the pH sensor. (a, i) The electrodes are coated in dopamine, which is polymerized into PDA using cyclic voltammetry (CV). These PDA-coated electrodes are the baseline pH sensors. (a, ii) The sensing mechanism of the PDA layer on the pH sensor when exposed to solutions with high and low pH. (b, i) Baseline pH sensors were modified with an (b, ii) 18 hour heat treatment at 100 °C, and (b, iii) by dip-coating them in agarose gel. These strategies were implemented to improve sensor stability.

rinsed with MilliQ water to remove the unpolymerized dopamine units and dried using a KimWipe, not touching the working, counter, or reference electrodes. The pH sensor was placed in a foil-wrapped petri dish and stored in an anoxic, UV-protective box until tested later in the day.

Heat treatment

A slightly modified protocol was followed to implement the thermal treatment.[28] Newly fabricated pH sensors were placed in a vacuum oven at 100 °C for 18 hours under humid conditions.

Agarose coating

3 wt% of agarose in 1× PBS was stirred in a 95 °C water bath until all agarose was dissolved. Next, the agarose mixture was placed in a 60 °C water bath and stirred for 30 minutes.[4] PDA-coated pH sensors were dipped halfway in the warm agarose solution for 3 seconds and left to dry for 1 minute. In total, each sensor was dipped in agarose five times. Those not immediately tested after fabrication were stored under dark, humid conditions.

Cyclic voltammetry (CV) testing

pH sensors were subjected to various CV scans in acetic acid, pH-corrected 1× PBS, and pH-corrected WFE. CV testing was performed using an 8-channel CH Instruments Electrochemical Analyzer (Austin, TX, USA). Each measurement comprised 1 CV cycle with a potential range between −0.2 V and 0.5 V at a scan rate of 0.05 V s^{-1} and a sampling interval of 0.005 V. A 5 minute wait period was applied before each measurement. The sensor's drift was calculated using the following equation. The oxidation potential (Epa) of the final scan was normalized with respect to the Epa of the initial scan.

$$\text{Drift } [\%] = \frac{\text{Epa}_{\text{final}}\ [\text{V}] - \text{Epa}_{\text{initial}}\ [\text{V}]}{\text{Epa}_{\text{initial}}\ [\text{V}]} \times 100\ [\%]$$

where $\text{Epa}_{\text{final}}$ [V] is the oxidation potential of the final scan in volts and $\text{Epa}_{\text{initial}}$ [V] is the oxidation potential of the initial scan in volts.

Polydopamine (PDA) detachment assay

The mass of the detached PDA was measured using the testing solutions of the baseline and heat-treated pH sensors after 30 CV scans. First, PBS solutions were spiked with different dopamine concentrations, and their optical densities were measured using an Agilent Biotek Synergy H1 Multimode Reader (Canada) at 280 nm (which is strongly absorbed by the benzene ring in dopamine) to create a calibration curve.[29] A nonlinear correlation was established between dopamine concentration and optical density (R^2 = 0.999, Fig. S1†). After performing 30 CV scans, the optical density of the testing solution on the electrodes was measured, and the result was interpolated using the calibration curve to find the mass of the detached PDA. The mass of detached PDA was not measured for the agarose-coated pH sensors because the testing solution had diffused through the agarose coating and could not be recovered.

Accuracy determination

pH-Corrected PBS and WFE were measured with the pH meter and the agarose-coated pH sensor. The pH readings obtained from the sensor were derived by interpolating the oxidation potential based on the calibration curve associated with the corresponding buffer. The accuracy percentage was calculated using the following equation.

$$\text{Accuracy } [\%] = \frac{\text{pH sensor}}{\text{pH meter}} \times 100\%$$

where pH sensor is the interpolated pH from the agarose-coated sensor and pH meter is the reading from the pH meter.

Results and discussion

Mechanism of pH sensing and validation of the pH sensor's response

pH sensors were fabricated by electrodepositing PDA on screen-printed gold electrodes *via* electrochemical CV scanning using previously established protocols.[26,27] The pH sensor is a 3-electrode system with gold working and counter electrodes and a silver/silver chloride reference electrode. Electrodeposition was used to coat the working electrode with PDA, a pH-responsive biopolymer composed of crosslinked dopamine. The electro-polymerization of dopamine undergoes various electron transfers and chemical reactions/isomerization to form the PDA layer. An electron transfer first converts dopamine to dopaminoquinone, which then undergoes a 1,4-Michael addition reaction resulting in leucodopaminochrome.[27] This substance further oxidizes into dopaminochrome.[27] The polymer deposition occurs after the final isomerization, redox reaction, and oxidation steps (ESI,† Scheme S1).[27] As more CV scans are completed, the thickness of the PDA coating increases.[27] The deposited PDA thin film has catechol moieties that are electrically oxidized into quinone moieties when subjected to CV scanning (Fig. 2a). The electrochemical potential at which the electro-oxidation happens, otherwise known as the oxidation peak or Epa, changes depending on the pH of the testing solution.[5,26,27,29] When exposed to a solution with a high pH, which contains a low concentration of H^+ ions, the oxidation of the catechol moieties into the quinone moieties is favorable; therefore, the Epa occurs at a lower potential. Meanwhile, when the pH sensor is exposed to a solution with a low pH, since it contains a high concentration of H^+ ions, the oxidation reaction is not as favorable. Thus, a larger potential is required to force the oxidation reaction to occur, as such the Epa increases. Therefore, the electrochemical

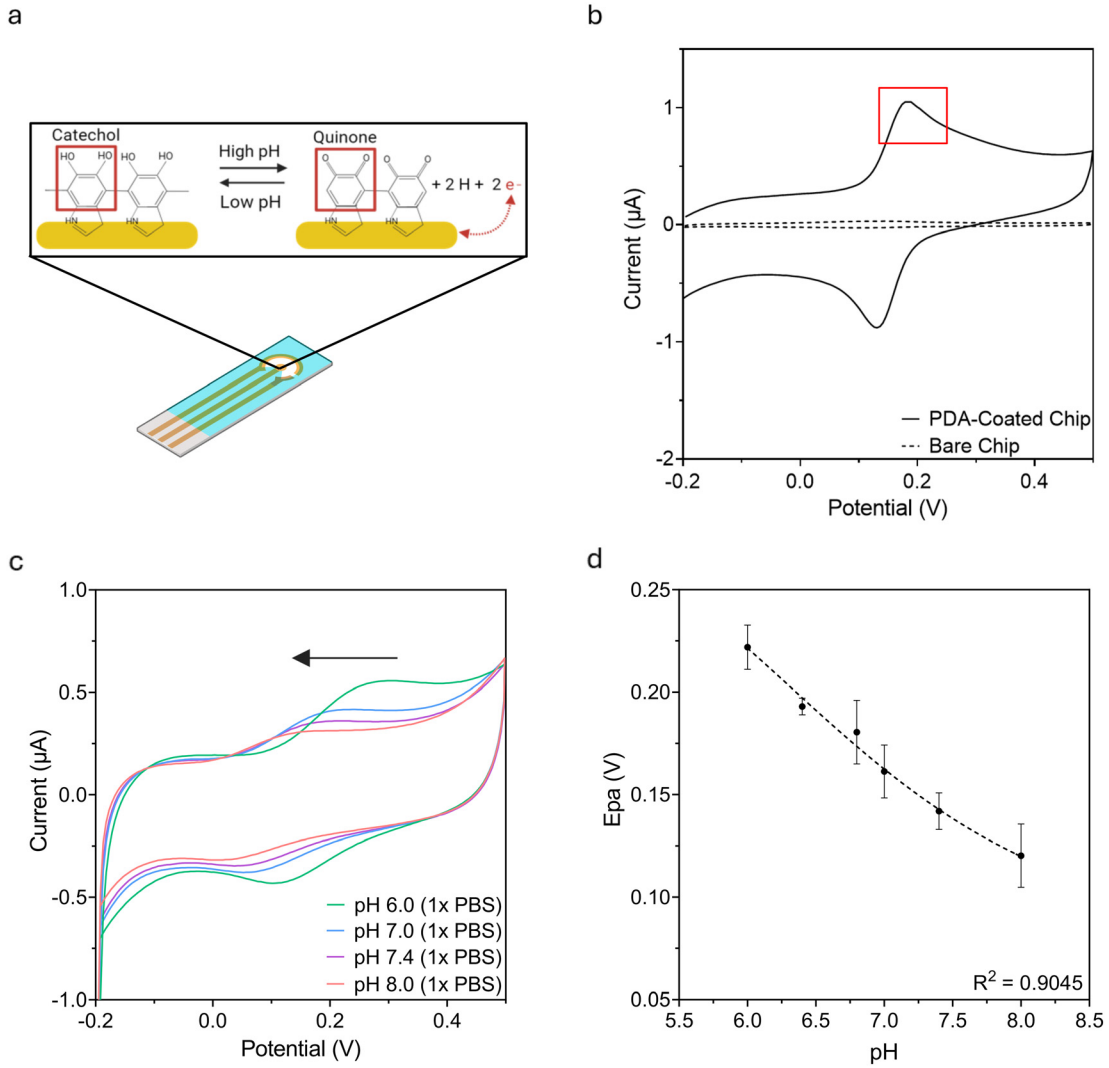

Fig. 2 Mechanism of pH sensing and validation of pH sensor response. (a) Schematic describing the pH sensing mechanism of the pH sensor. (b) CV of a bare gold electrode (dashed line) and pH sensor (solid line) tested in acetic acid at pH 5.0. The oxidation peak of the PDA-coated pH sensor is boxed in red, and no relevant peak is observed for the bare electrode. (c) The CV scans of the pH sensor in PBS with varying pH. (d) Corresponding logarithmic calibration curve of pH sensors ($n \geq 4$) tested in PBS with varying pH (R^2 = 0.904, sensitivity = slope of the linear region [6.0–7.0] = −0.06 V pH^{-1}). Error bars represent the standard deviation (STD). All CV scans were conducted in a potential range between −0.2 V and 0.5 V, a scan rate of 0.05 V s^{-1}, and a sampling interval of 0.005 V. The schematic was created using BioRender.

potential of the PDA oxidation or the Epa can indicate the pH of the solution.

The success of the PDA electrodeposition was confirmed using CV in acetic acid solution (pH 5.0). Fig. 2b shows the voltammetric behavior of a bare gold electrode (dashed line) and a PDA-coated pH sensor (solid line) in response to acetic acid solution (pH 5.0). The pH sensor has a strong Epa near 0.25 V, which is associated with the oxidation of the catechol moieties of dopamine.[26,27] The bare gold electrode does not show the voltammetric response, confirming the successful deposition of PDA. The small peaks observed near 0.07 and −0.07 are likely caused by impurities present in the environment.[30]

The PDA-coated pH sensors were tested with 1× PBS solution of varying clinically relevant pH ranging from 6.0–8.0 to examine the sensor's response (Fig. 2c). The pH 6.0 buffer showed an Epa near 0.22 V, while the Epa of pH 8.0 buffer was near 0.09 V. As the pH of solutions increased, the Epa peaks followed the expected trend and shifted to lower potentials. The increase of Epa was correlated with the decrease in pH (R^2 = 0.904, Fig. 2d). The sensitivity of the pH sensor is defined as the slope of the linear region between pH 6.0–7.0 and was found to be −0.06 V pH^{-1}.

Validating the stability of the pH sensor in response to multiple scans

The measure of body fluid's pH can be used for early detection of infection and health complications.[31] pH can provide valuable information on the wound healing process,

can be used to diagnose chronic illnesses such as gastroesophageal reflux disease, and can be utilized to monitor organ function, such as the kidneys' ability to remove acid from the blood.[31–33] Particularly, continuous pH monitoring is highly beneficial in showing trends that discrete points might miss, enabling timely interventions. Studies have shown that continuous pH monitoring can help detect anastomotic leaks post-surgical intervention, identify infection in chronic wounds, and monitor illnesses related to acid/base imbalances, such as ischemia.[2,34,35]

To investigate the suitability of the developed pH sensor for continuous measurements, we tested its stability over several scans. The pH sensors were subjected to 30 scans in 1× PBS buffer solution with pH 7.3 (Fig. 3a). From scan 1 to scan 30, the baseline pH sensors experienced a 60.8% decrease in Epa, with the most considerable drift occurring within the first ten scans (Fig. 3b). The inset of Fig. 3b illustrates the corresponding CV measurements at scan 1 and scan 30 with the Epa outlined in red. The Epa shifts towards left between the first and last scan (Fig. 3b).

Previous studies have shown that thermal annealing has enhanced the mechanical performance of PDA films due to further polymerization of the oligo dopamine units, strengthening intermolecular interactions.[28,36] To improve mechanical stability, newly coated PDA pH sensors were annealed in an oven at 100 °C for 18 hours in a Petri dish wrapped with tin foil and Parafilm. A KimWipe saturated with DI water was placed in the Petri dish during the annealing process to maintain humid conditions. Annealed sensors were subjected to 30 CV scans in a buffer with pH 7.3 (Fig. 3c). Between scan 1 and scan 30, the heat-treated pH sensors experienced an average Epa decrease of 44.8%

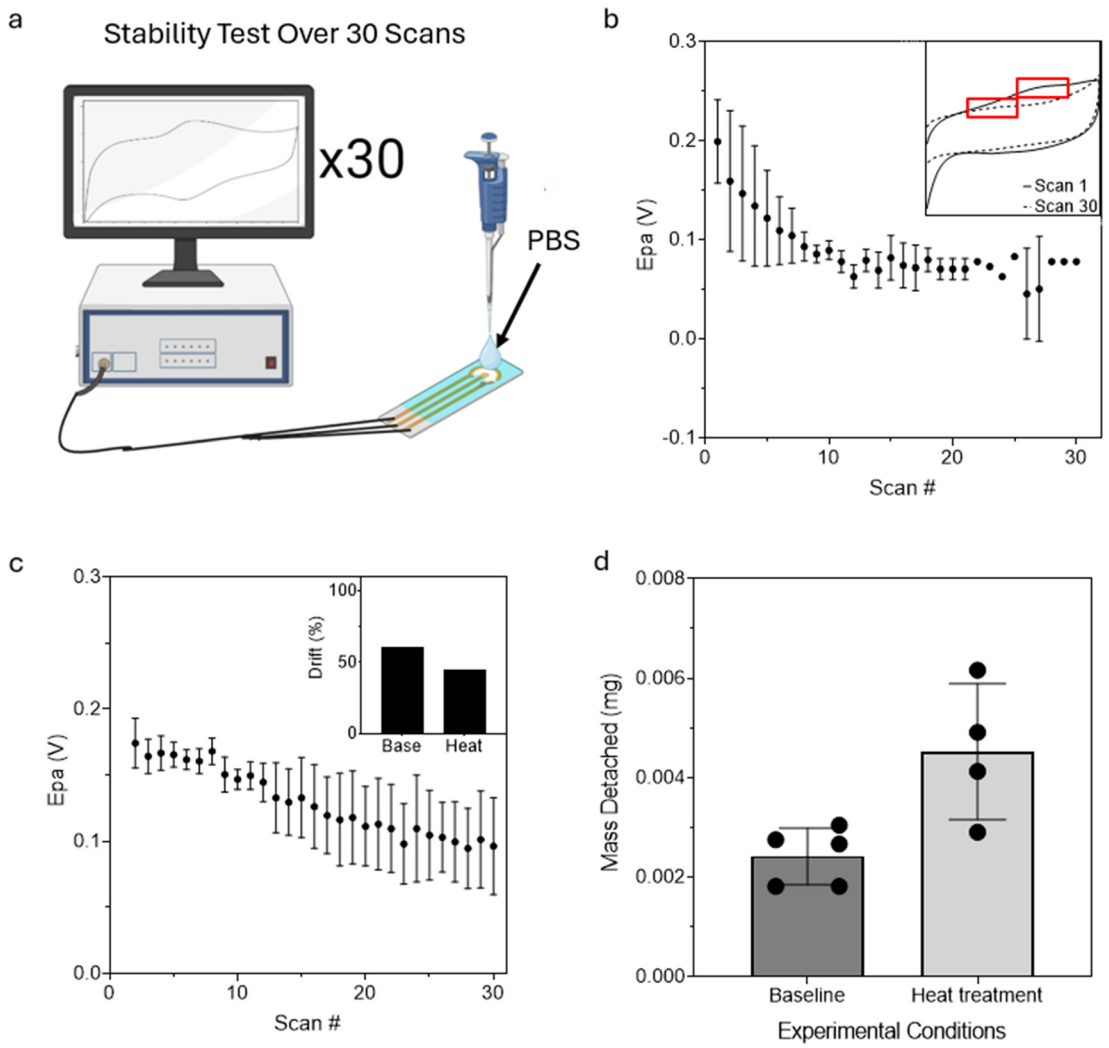

Fig. 3 Validating the stability of the pH sensor in response to multiple scans. (a) Schematic illustration of the CV scanning protocol for testing the stability of pH sensors. (b) Corresponding oxidation potential of the pH sensors ($n \geq 4$) at pH 7.3 over 30 scans. The inset displays the CV measurements for scan 1 and scan 30. (c) Corresponding oxidation potential of the heat-treated pH sensors ($n \geq 4$) at pH 7.3 over 30 scans. The inset shows the signal drift measured between scan 1 and scan 30 for the baseline and heat-treated pH sensors. (d) The amount of PDA detached from the pH sensors ($n \geq 4$) after the 30th scan with and without heat treatment. Error bars represent the STD. The schematic was created using BioRender.

(Fig. 3c inset), with the most considerable drift occurring between scan 10 and scan 20. After scan 12, a major drift was observed, suggesting that the heat treatment only increased stability for the first 10 scans. Fig. S2† displays the changes observed in the CVs measured for scan 1 and scan 30. The Epa had shifted left between the first and last scan.

We designed and performed a study to investigate whether the heat treatment had led to stronger PDA attachment. pH sensors were prepared with and without heat treatment and 30 CV scans were performed on each sensor. The buffer in which the scans were performed was collected to measure the amount of released PDA (Fig. 3d and S1†). The optical density of the testing solution was measured and then correlated with the mass of the detached PDA (Fig. 3d and S1†). Despite our expectations, the collected buffer from the heat-treated pH sensors showed higher amounts of detached PDA than the baseline pH sensors (Fig. 3d). Heat treatment reduces the number of amine groups in the PDA coating, which can make the surface more hydrophobic.[28,29] When the hydrophobic, heat-treated PDA coating is exposed to an aqueous solution, the PDA would form aggregates, detaching from the hydrophilic gold electrode surface.[37] Additionally, PDA heat treatment might increase the number of quinone moieties, which could negatively impact the pH sensor's performance.[29] The increase in quinone units can reduce the pH response and sensitivity, as the pH response is dependent on the oxidation of the catechol moieties of PDA to quinone

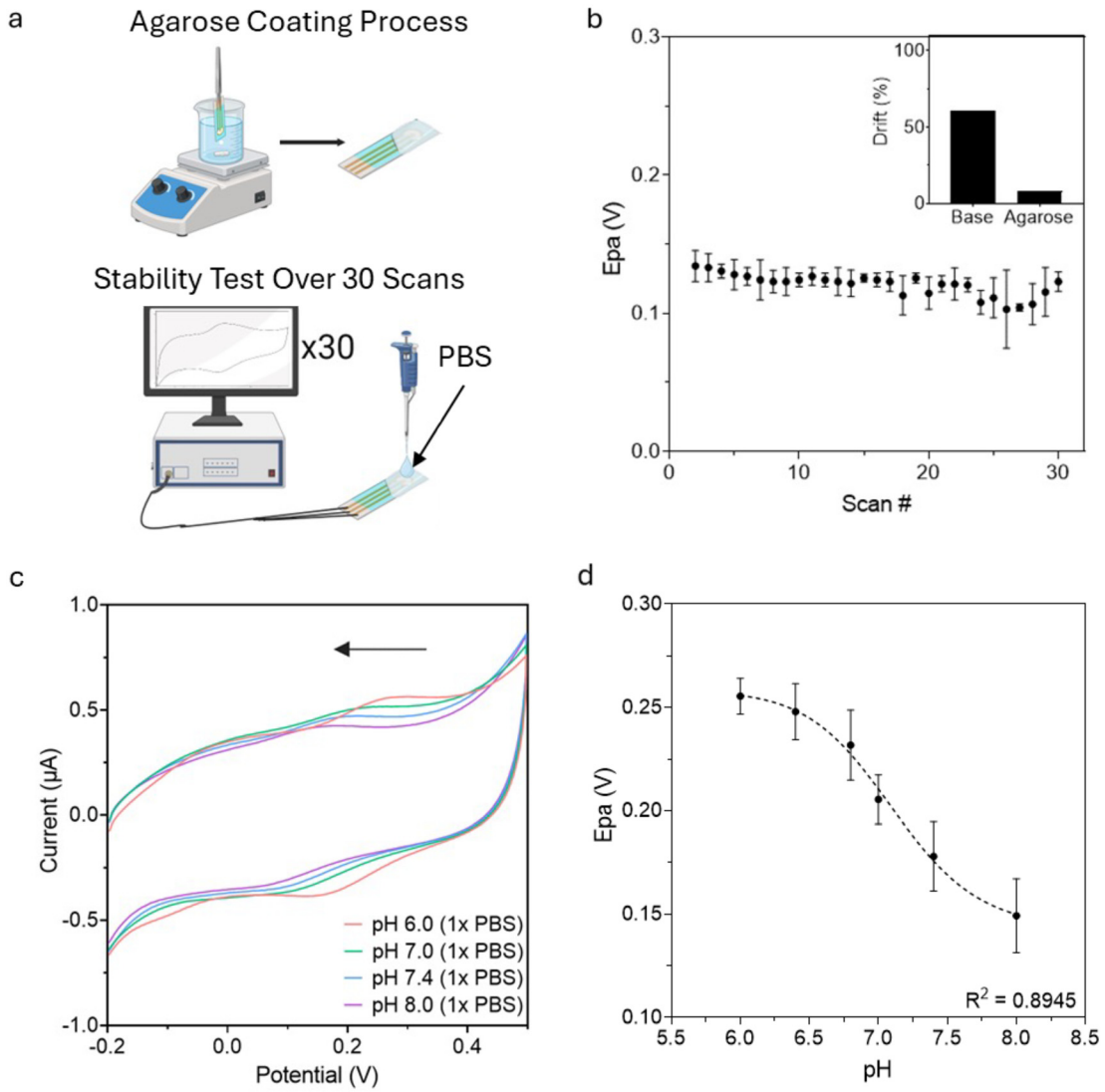

Fig. 4 Utilizing agarose gel to improve pH sensor stability. (a) Schematic showing the process for agarose coating and the following stability test *via* CV scanning. (b) Oxidation potentials of pH sensors ($n \geq 4$) coated with agarose over 30 scans. The inset shows the signal drift measured between scan 1 and scan 30 for the baseline and agarose-coated pH sensors. (c) Representative CVs of an agarose-coated pH sensor tested in PBS with varying pH. (d) Corresponding calibration curve of pH sensors ($n \geq 4$) tested with varying pH (R^2 = 0.894, sensitivity = slope of the linear region [6.4–7.4] = −0.06 V pH^{-1}). Error bars represent the STD. All CV scans were conducted in a potential range between −0.2 V and 0.5 V, a scan rate of 0.05 V s^{-1}, and a sampling interval of 0.005 V.

moieties.[28] As stated, our data indicates that although heat treatment decreases the percentage change from 60.8% to 44.8%, there is still a 44.8% decrease in the response, requiring strategies that achieve a more stable signal (Fig. 3c inset).

Utilizing agarose gel coating to improve pH sensor stability

Hydrogels are crosslinked polymer chains that form insoluble networks. Due to their biocompatibility, they have been used in contact lenses, bio-adhesives, drug delivery, and marine antifouling coatings.[38,39] Known for their hydrophilicity and significant water content, they mimic biological tissue and have thus been used to coat implantable electrodes.[38] They also possess antifouling properties.[39] Hydrogels are popular due to their diffusive properties, which allow the passage of aqueous solutions and molecules through their pores by size filtering, electrostatic forces, hydrogen bonds, and specific binding.[40] Agarose gel is a naturally occurring, anionic, polysaccharide hydrogel harvested from algae and has been used as an electrode coating to improve the stability of aptamer-based electrochemical biosensors.[4]

To explore the stabilization properties of agarose for pH sensors, we coated fabricated pH sensors with agarose and examined its durability over multiple scans. The pH sensor was dip-coated in agarose and subsequently subjected to 30 scans in PBS buffer with pH 7.3 (Fig. 4a). Between the first and last scan, the agarose-coated pH sensors experienced an 8.2% decrease in Epa, which is significantly improved compared to the 60.8% decrease observed from the baseline pH sensors (Fig. 4b). Fig. S3† displays the CV measurements at scan 1 (solid line) and scan 30 (dashed line) and highlights the minimal shift of Epa. The success of the agarose coating in minimizing the drift in sensor response can be attributed to its acting as a protective layer for the PDA and confining it to the electrode surface.[4] The agarose layer also minimizes the passage and accumulation of large molecules, thus potentially protecting the PDA from lifting due to fouling when subject to complex body fluids.[4] In the absence of agarose, aggregates could form from large molecules binding to the PDA, which could cause the PDA layer to detach from the electrode surface.[41] Further, agarose can also limit the PDA layer's exposure to air, preventing its overoxidation.[42]

The pH response of the agarose-coated pH sensors was also tested in a pH range between 6.0 and 8.0 (Fig. 4c). As the solutions' pH increased, the Epa peaks shifted to lower potentials, following the expected trend (Fig. 4c). The Epa decrease and pH increase were found to be correlated with an R^2 of 0.894 (Fig. 4d). The sensor's sensitivity is defined as the slope of the fitted line in the linear region between pH 6.4 and 7.4 and was found to be −0.06 V pH^{-1}.

The developed pH sensor can have a wide range of clinical applications, including early tumour screening *via* tracking interstitial fluid pH,[43,44] assisting in diagnosing urinary tract infections,[45] and monitoring infections in chronic wounds.[12,13]

The physiological pH of ISF is 7.35–7.45,[44,46] but ISF lacks a strong buffering capacity, allowing its pH to shift more easily.[44] Tumour presence, for instance, can lower ISF pH to around 6.2.[44,47] Therefore, the agarose-coated pH sensor could serve as a preliminary ISF screening tool by detecting significant deviations from normal pH levels.

The developed pH sensor can also be implemented to detect pH changes in urine.[45] The physiological pH of urine is 6.2 but may differ following an infection.[48] In the presence of some common bacteria which cause urinary tract infections, the urine pH rises to about 6.72.[48] The developed pH sensor can detect this pH difference as it lies within its dynamic range.

The pH sensor can also detect the pH changes in wound fluid caused by chronic infections. The physiological pH of wound fluid is typically around 6.[12,13] When the wound is infected, the pH of wound fluid increases to pH 7–9.[12,13] The developed pH sensor could effectively detect the differences in wound fluid's physiological and pathological pH.

Testing pH sensor stability in a complex biological fluid

We further tested the stability of the pH sensor in simulated wound fluid exudate (WFE) to assess the efficacy of the pH sensor in a complex fluid, both with and without the agarose coating. The uncoated pH sensor underwent 30 scans in WFE with a pH of 7.32 (Fig. S4a†). The pH sensor exhibited a 75% drift in Epa between the first and last scans. This significant drift is likely attributed to the complexity of WFE, as it contains significant amounts of proteins, particularly bovine serum albumin (BSA).[49] These proteins can lead to non-specific binding on the electrode, thereby increasing the observed drift.[4,50] Additionally, the drift may have been influenced by the overoxidation of the PDA surface.[42] Furthermore, large aggregates or molecules could have adhered to the PDA, potentially causing the PDA layer to detach from the sensor surface and affecting the sensor's response.[41] The corresponding calibration curve for the pH sensor in WFE yielded an R^2 value of 0.98 and a sensitivity of −0.08 in the linear region between pH of 6.0 and 7.0 (Fig. S4b†). Fig. S5† presents the CV measurements taken at scan 1 (solid line) and scan 30 (dashed line), clearly showcasing the substantial shift in Epa. The pH response of the sensors was evaluated, which showed the expected trend: Epa decreased with increasing pH.

We then tested the stability of the agarose-coated pH sensors in WFE to explore the coating's efficacy in minimizing signal drift in a more complex fluid (Fig. 5a). The agarose-coated pH sensor was subjected to 30 scans in WFE at pH 7.32 (Fig. 5b). The sensor showed an Epa drift of 8.3%, which is significantly lower than the 75% drift seen with the uncoated pH sensor. This demonstrates the efficacy of the agarose coating in enhancing the stability of pH sensor in complex fluids. The reduced drift may be attributed to the coating's anti-fouling properties, which decrease the accumulation of proteins in the WFE on the sensor

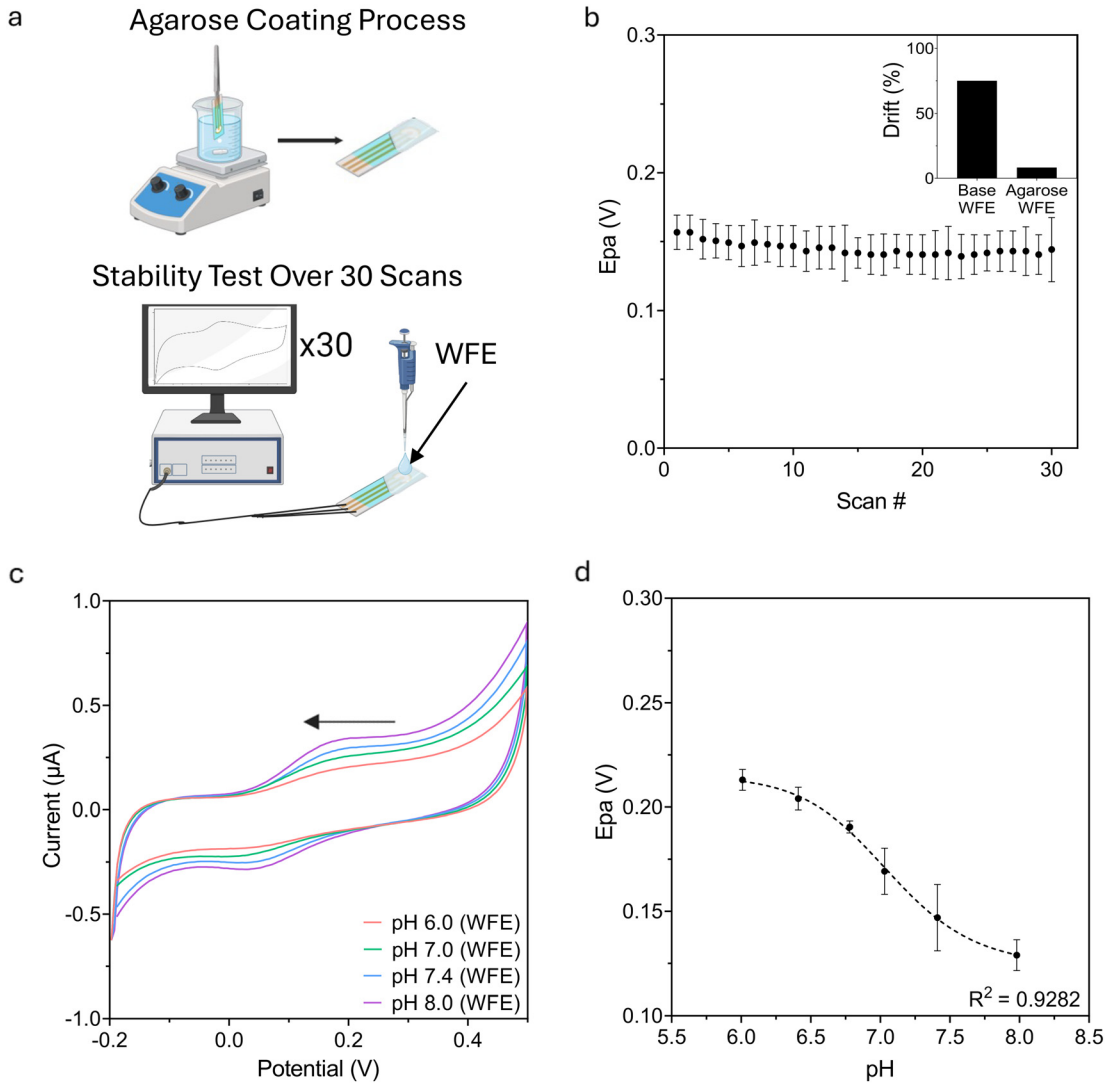

Fig. 5 Testing the pH sensor and agarose-coated pH sensor in a complex biological fluid. (a) Schematic showing the process for agarose coating and the following stability test *via* CV scanning in simulated wound fluid (WFE). (b) Oxidation potentials of pH sensors (n = 4) coated with agarose over 30 scans in WFE. The inset shows the signal drift measured between scan 1 and scan 30 for the baseline and agarose-coated pH sensors. (c) Representative CVs of an agarose-coated pH sensor tested in WFE of varying pH. (d) Corresponding calibration curve of pH sensors (n = 4) tested with varying pH (R^2 = 0.92, sensitivity = slope of the linear region [6.4–7.4] = −0.06). Error bars represent the STD.

surface.[4,50] The minimal drift observed between scan 1 (solid line) and scan 30 (dashed line) is presented in Fig. S6.† The pH response of the agarose-coated pH sensor was also evaluated, and the expected trend was observed (Fig. 5c). The resulting calibration curve for the agarose-coated pH sensor in WFE had an R^2 value of 0.93 and a sensitivity of −0.06 in the linear region between pH 6.4 and 7.4 (Fig. 5d).

The accuracy of the agarose-coated pH sensor was acquired by calculating the percentage ratio between the pH measured using the pH sensor and the commercial pH meter (Table 1). The agarose-coated pH sensor demonstrated an accuracy percentage of 100.14% in WFE, 101.15% in PBS with pH 7.31, and 101.15% in PBS with pH 7.4.

Conclusion

In this work, we fabricated a pH sensor based on the electrodeposition of polydopamine on the surface of a gold

Table 1 Accuracy comparison of an agarose-coated pH sensor in PBS and WFE

Fluid	Mean pH (measured with agarose-coated pH sensor)	Mean pH (measured with pH meter)	Mean accuracy [%]	StanDev	Replicates [n]
PBS	7.40	7.31	101.26	1.181	3
PBS	7.485	7.4	101.15	0.00	3
WFE	7.25	7.32	100.14	1.524	3

electrode and tested its performance in response to varying pH in both PBS and WFE. Since the continuous measurement of pH is critical for monitoring organ function, disease progression, and wound healing processes, we further explored the stability of the pH sensor over several continuous measurements. We observed a major drift when testing the baseline PDA sensor as it presented a 60.8% decrease in the signal by the 30th scan in PBS, and a 75% drift in the signal by the 30th scan in WFE, thus failing to provide stable continuous sensing. We tested two strategies to improve sensor stability: heat treatment and agarose-coating. We evaluated the stability of the modified sensors by subjecting them to 30 consecutive scans. Implementing an 18 hour heat treatment led to a 44.8% drift in the pH sensor's response, yet it was still not stable enough for continuous sensing. The agarose-coating strategy greatly improved the stability of the obtained signals, as the 30th scan observed only an 8.2% drift in the signal in PBS, and an 8.3% drift in the signal in WFE. The result of each scan during the stability testing can possibly be used as an analog to pH measurements executed in a clinical environment. For instance, our findings suggest that if two pH measurements are taken daily, the agarose-coated pH sensor can potentially provide stable and accurate results for 15 days. However, further testing is needed to confirm the sensor's efficacy in human bodily fluids for clinical use.

The possible clinical applications of the agarose-coated pH sensor include monitoring pH both *in vivo* and *ex vivo*. The sensor could be integrated into various medical devices and implemented for clinical applications to streamline treatment in hospitals and outpatient clinics.[5] For instance, the pH sensor can be integrated into microneedles to enable minimally invasive transdermal pH sensing, which can screen for tumour occurrence.[35,44,47] The pH sensor can also be integrated into catheters to continuously monitor urine pH to assist with the detection of urinary tract infections,[48] and monitor blood pH to observe the progression of hypoxia, as blood pH increases with elevated carbon dioxide levels.[51] The pH sensor can also be applied as part of a wound dressing to monitor wound fluids for infection.[52] Further *in vivo* and *ex vivo* testing in other study models and animals would, in turn, prepare the pH sensor for human implementation.

Future work can focus on longer testing durations to further determine the effectiveness of the agarose coating for long-term stability, as prior research shows the possibility of long-term stability for up to seven days.[4] The presented work tested the pH sensor in 1× PBS and simulated WFE, yet conducting future experiments in an array of biological fluids would help to explore the efficacy of agarose's long-term stability and antifouling effects.

Data availability

The data supporting the results in this study are available within the manuscript and its ESI.† Further information can be inquired from the corresponding author *via* e-mail.

Author contributions

Natalie Fudge, and Joshua Khatri performed the experiments. Natalie Fudge, Fatemeh Keyvani, and Joshua Khatri designed the experiments and analyzed the data. Natalie Fudge, Fatemeh Keyvani, Joshua Khatri, and Mahla Poudineh discussed the findings. Natalie Fudge, Fatemeh Keyvani, and Mahla Poudineh contributed to manuscript writing and editing.

Conflicts of interest

There are no conflicts to declare.

Acknowledgements

Schematics were created in BioRender, and chemical structures were drawn in ChemSketch. This research was supported by Waterloo CBB seed funding. The authors like to acknowledge the Natural Sciences and Engineering Research Council of Canada for providing financial support to Fatemeh Keyvani (the Canada graduate scholarship-doctorate program) as well as Natalie Fudge and Joshua Khatri (the undergraduate student research award stream) during the course of study.

References

1 C. Wang, T. He, H. Zhou, Z. Zhang and C. Lee, Artificial intelligence enhanced sensors - enabling technologies to next-generation healthcare and biomedical platform, *Bioelectron. Med.*, 2023, **9**, 17.
2 M. Huynh, R. Tjandra, N. Helwa, M. Okasha, A. El-Falou and Y. Helwa, Continuous pH monitoring using a sensor for the early detection of anastomotic leaks, *Front. Med. Technol.*, 2023, **5**, 1128460.
3 D. Olczuk and R. Priefer, A history of continuous glucose monitors (CGMs) in self-monitoring of diabetes mellitus, *Diabetol. Metab. Syndr.*, 2018, **12**, 181–187.
4 S. Li, J. Dai, M. Zhu, N. Arroyo-Currás, H. Li and Y. Wang, *et al.*, Implantable Hydrogel-Protective DNA Aptamer-Based Sensor Supports Accurate, Continuous Electrochemical Analysis of Drugs at Multiple Sites in Living Rats, *ACS Nano*, 2023, **17**(18), 18525–18538.
5 M. Hassan Akhtar, M. Azhar Hayat Nawaz, M. Abbas, N. Liu, W. Han and Y. Lv, *et al.*, Advances in pH Sensing: From Traditional Approaches to Next-Generation Sensors in Biological Contexts, *Chem. Rec.*, 2024, **24**(7), e202300369.
6 W. B. Fye, A History of the Origin, Evolution, and Impact of Electrocardiography, *J. Cardiol.*, 1995, **73**(13), 937–949.
7 M. Tabata, C. Khamhanglit, S. Kotaki and Y. Miyahara, Detection of cell membrane proteins using ion-sensitive field effect transistors combined with chemical signal amplification, *Chem. Commun.*, 2022, **58**(53), 7368–7371, available from: **https://pubs.rsc.org/en/content/articlehtml/2022/cc/d2cc02159e**.
8 T. Abbasiasl, F. Mirlou, H. Mirzajani, M. J. Bathaei, E. Istif and N. Shomalizadeh, *et al.*, A Wearable Touch-Activated Device Integrated with Hollow Microneedles for Continuous

Sampling and Sensing of Dermal Interstitial Fluid, *Adv. Mater.*, 2024, **36**(2), 2304704, DOI: **10.1002/adma.202304704**.
9 T. Hickish and A. D. Farmery, Acid–base physiology, *Anaesth. Intensive Care Med.*, 2021, **22**, 422–427.
10 M. T. Ghoneim, A. Nguyen, N. Dereje, J. Huang, G. C. Moore and P. J. Murzynowski, *et al.*, Recent Progress in Electrochemical pH-Sensing Materials and Configurations for Biomedical Applications, *Chem. Rev.*, 2019, **119**(8), 5248–5297, available from: **https://pubs.acs.org/sharingguidelines**.
11 J. H. Yoon, S. M. Kim, H. J. Park, Y. K. Kim, D. X. Oh and H. W. Cho, *et al.*, Highly self-healable and flexible cable-type pH sensors for real-time monitoring of human fluids, *Biosens. Bioelectron.*, 2020, **150**, 111946.
12 P. Yang, Z. Zhu, T. Zhang, W. Zhang, W. Chen and Y. Cao, *et al.*, Orange-Emissive Carbon Quantum Dots: Toward Application in Wound pH Monitoring Based on Colorimetric and Fluorescent Changing, *Small*, 2019, **15**(44), 1902823, DOI: **10.1002/smll.201902823**.
13 S. Zhang, L. Wang, T. Xu and X. Zhang, Luminescent MOF-Based Nanofibers with Visual Monitoring and Antibacterial Properties for Diabetic Wound Healing, *ACS Appl. Mater. Interfaces*, 2022, **15**(7), 9110–9119.
14 V. Krivenkov, Y. P. Rakovich, P. Samokhvalov and I. Nabiev, pH-Sensing Platform Based on Light-Matter Coupling in Colloidal Complexes of Silver Nanoplates and J-Aggregates, *J. Phys. Chem. C*, 2021, **125**(3), 1972–1979, DOI: **10.1021/acs.jpcc.0c10602**.
15 A. Steinegger, O. S. Wolfbeis and S. M. Borisov, Optical Sensing and Imaging of pH Values: Spectroscopies, Materials, and Applications, *Chem. Rev.*, 2020, **120**(22), 12357–12489, DOI: **10.1021/acs.chemrev.0c00451**.
16 Y. Sasaki, X. Lyu and T. Minami, A Highly Accurate pH Detection Method for Sweat Analysis using a Printed 96-Microwell Colorimetric Sensor Array, *Analysis Sensing*, 2023, **3**(5), e202200097, DOI: **10.1002/anse.202200097**.
17 M. Zea, R. Texidó, R. Villa, S. Borrós and G. Gabriel, Specially Designed Polyaniline/Polypyrrole Ink for a Fully Printed Highly Sensitive pH Microsensor, *ACS Appl. Mater. Interfaces*, 2021, **13**(28), 33524–33535, DOI: **10.1021/acsami.1c08043**.
18 J. X. Zhou, F. Ding, L. N. Tang, T. Li, Y. H. Li and Y. J. Zhang, *et al.*, Monitoring of pH changes in a live rat brain with MoS2/PAN functionalized microneedles, *Analyst*, 2018, **143**(18), 4469–4475, available from: **https://pubs.rsc.org/en/content/articlehtml/2018/an/c8an01149d**.
19 C. Y. Hsieh and N. T. Huang, A proton-selective membrane (PSM)-deposited dual-gate ion-sensitive field-effect transistor (DG-ISFET) integrating a microchamber-embedded filter membrane for bacterial enrichment and antimicrobial susceptibility test, *Sens. Actuators, B*, 2022, **359**, 131580.
20 B. Y. Sun, W. H. Cheang, S. C. Chou, J. C. Chiao and P. W. Wu, Fabrication of Cu Micromembrane as a Flexible Electrode, *Nanomaterials*, 2022, **12**(21), 3829, available from: **https://pmc.ncbi.nlm.nih.gov/articles/PMC9654814/**.
21 S. Casans, D. R. Muñoz, A. E. Navarro and A. Salazar, ISFET drawbacks minimization using a novel electronic compensation, *Sens. Actuators, B*, 2004, **99**(1), 42–49.
22 K. M. Chang, C. T. Chang, K. Y. Chao and C. H. Lin, A Novel pH-dependent Drift Improvement Method for Zirconium Dioxide Gated pH-Ion Sensitive Field Effect Transistors, *Sensors*, 2010, **10**, 4643–4654, available from: **https://www.mdpi.com/1424-8220/10/5/4643/htm**.
23 V. Prathap and A. H. Titus, A differential p-ISFET based on-chip pH sensor with substrate based drift reset capability, *Proc. IEEE Sens.*, 2021, 9639844.
24 J. C. Chou, H. M. Tsai, C. N. Shiao and J. S. Lin, Study and simulation of the drift behaviour of hydrogenated amorphous silicon gate pH-ISFET, *Sens. Actuators, B*, 2000, **62**(2), 97–101.
25 C. Rundle and H. Kreuzberg, *Glossary of Terms and Calculations used in Ion Selective Electrode Measurements*, Nico2000 Ltd., 1999.
26 M. Amiri, E. Amali, A. Nematollahzadeh and H. Salehniya, Poly-dopamine films: Voltammetric sensor for pH monitoring, *Sens. Actuators, B*, 2016, **228**, 53–58.
27 J. Szewczyk, D. Aguilar-Ferrer and E. Coy, Polydopamine films: Electrochemical growth and sensing applications, *Eur. Polym. J.*, 2022, **174**, 111346.
28 M. B. Davidsen, J. F. L. Teixeira, J. Dehli, C. Karlsson, D. Kraft and P. P. C. Souza, *et al.*, Post-treatments of polydopamine coatings influence cellular response, *Colloids Surf., B*, 2021, **207**, 111972.
29 H. Wei, J. Ren, B. Han, L. Xu, L. Han and L. Jia, Stability of polydopamine and poly(DOPA) melanin-like films on the surface of polymer membranes under strongly acidic and alkaline conditions, *Colloids Surf., B*, 2013, **110**, 22–28.
30 E. Bernalte, C. Marín-Sánchez, E. Pinilla-Gil and C. M. A. Brett, Characterisation of screen-printed gold and gold nanoparticle-modified carbon sensors by electrochemical impedance spectroscopy, *J. Electroanal. Chem.*, 2013, **709**, 70–76.
31 S. H. Kuo, C. J. Shen, C. F. Shen and C. M. Cheng, Role of pH value in clinically relevant diagnosis, *Diagnostics*, 2020, **10**, 10020107.
32 G. M. Kamphuis, J. W. Van Hattum, P. De Bie and B. K. Somani, Method of alkalization and monitoring of urinary pH for prevention of recurrent uric acid urolithiasis: A systematic review, *Transl. Androl. Urol.*, 2019, **8**, S448–S456.
33 O. Korostynska, K. Arshak, E. Gill and A. Arshak, Review Paper: Materials and techniques for in vivo pH monitoring, *IEEE Sens. J.*, 2008, **8**, 20–28.
34 N. Pan, J. Qin, P. Feng, Z. Li and B. Song, Color-changing smart fibrous materials for naked eye real-time monitoring of wound pH, *J. Mater. Chem. B*, 2019, **7**(16), 2626–2633.
35 J. J. García-Guzmán, C. Pérez-Ràfols, M. Cuartero and G. A. Crespo, Toward in Vivo Transdermal pH Sensing with a Validated Microneedle Membrane Electrode, *ACS Sens.*, 2021, **6**(3), 1129–1137.
36 K. G. Malollari, P. Delparastan, C. Sobek, S. J. Vachhani, T. D. Fink and R. H. Zha, *et al.*, Mechanical Enhancement of

Bioinspired Polydopamine Nanocoatings, *ACS Appl. Mater. Interfaces*, 2019, **11**(46), 43599–43607.
37 Q. Sun, The Hydrophobic Effects: Our Current Understanding, *Molecules*, 2022, **27**, 7009.
38 R. A. Green, S. Baek, L. A. Poole-Warren and P. J. Martens, Conducting polymer-hydrogels for medical electrode applications, *Sci. Technol. Adv. Mater.*, 2010, **11**, 014107.
39 D. Su, X. Bai and X. He, Research progress on hydrogel materials and their antifouling properties, *Eur. Polym. J.*, 2022, **181**, 111665.
40 O. Lieleg and K. Ribbeck, Biological hydrogels as selective diffusion barriers, *Trends Cell Biol.*, 2011, **21**, 543–551.
41 A. Gélinas, M. Laurent and G. Laroche, Electrode cleanliness impact on the surface treatment of fluoropolymer films for a long-lasting plasma process, *Manuf. Lett.*, 2020, **26**, 1–5.
42 O. Ben-Zvi, I. Grinberg, A. A. Orr, D. Noy, P. Tamamis and I. Yacoby, *et al.*, Protection of Oxygen-Sensitive Enzymes by Peptide Hydrogel, *ACS Nano*, 2021, **15**(4), 6530–6539.
43 Z. Wu, Z. Qiao, S. Chen, S. Fan, Y. Liu and J. Qi, *et al.*, Interstitial fluid-based wearable biosensors for minimally invasive healthcare and biomedical applications, *Commun. Mater.*, 2024, **5**(1), 1–15, available from: **https://www.nature.com/articles/s43246-024-00468-6**.
44 M. Dervisevic, E. Dervisevic, L. Esser, C. D. Easton, V. J. Cadarso and N. H. Voelcker, Wearable microneedle array-based sensor for transdermal monitoring of pH levels in interstitial fluid, *Biosens. Bioelectron.*, 2023, **222**, 114955.
45 M. Merz, Y. Ponomarev and R. Pijnenburg, Sensor module for a catheter, US8233957B2, 2024, available from: **https://patents.google.com/patent/US8233957B2/en**.
46 I. Torres-Terán, M. Venczel and S. Klein, Prediction of subcutaneous drug absorption - do we have reliable data to design a simulated interstitial fluid?, *Int. J. Pharm.*, 2021, **610**, 121257.
47 R. K. Jain, S. A. Shah and P. L. Finney, Continuous Noninvasive Monitoring of pH and Temperature in Rat Walker 256 Carcinoma During Normoglycemia and Hyperglycemia, *J. Natl. Cancer Inst.*, 1984, **73**, 429–436.
48 H. C. Lai, S. N. Chang, H. C. Lin, Y. L. Hsu, H. M. Wei and C. C. Kuo, *et al.*, Association between urine pH and common uropathogens in children with urinary tract infections, *J. Microbiol., Immunol. Infect.*, 2021, **54**(2), 290–298.
49 I. Sangita, S. Vishwanath, K. Sadasiva, A. Ramachandran, Y. Thanikachalam and V. Ramya, Influence of Simulated Wound Exudate on the Antimicrobial Efficacy of Various Intracanal Medicaments Against Enterococcus faecalis: An In Vitro Study, *Cureus*, 2023, **15**(5), 38677.
50 J. Sabaté del Río, O. Y. F. Henry and P. Jolly, Ingber DE. An antifouling coating that enables affinity-based electrochemical biosensing in complex biological fluids, *Nat. Nanotechnol.*, 2019, **14**(12), 1143–1149, available from: **https://www.nature.com/articles/s41565-019-0566-z**.
51 T. Yoshida, M. Udo, M. Chida and K. Makiguchi, Effect of hypoxia on arterial and venous blood levels of oxygen, carbon dioxide, hydrogen ions and lactate during incremental forearm exercise, *Eur. J. Appl. Physiol. Occup. Physiol.*, 1989, **58**, 772–777.
52 F. Mariani, M. Serafini, I. Gualandi, D. Arcangeli, F. Decataldo and L. Possanzini, *et al.*, Advanced Wound Dressing for Real-Time pH Monitoring, *ACS Sens.*, 2021, **6**(6), 2366–2377, DOI: **10.1021/acssensors.1c00552**.